Materials Horizons

ROYAL SOCIETY OF CHEMISTRY

COMMUNICATION

View Article Online
View Journal | View Issue

Cite this: *Mater. Horiz.*, 2025, 12, 487

Received 29th August 2024,
Accepted 15th October 2024

DOI: 10.1039/d4mh01172d

rsc.li/materials-horizons

Electrothermally powered synergistic fluorescence-colour/3D-shape changeable polymer gel systems for rewritable and programmable information display†

Junni Xie,‡[ab] Chaojun Yue,‡[ac] Shaohuang Chen,*[d] Zhenyi Jiang,[ab] Shuangshuang Wu,[ab] Weiqing Yang,[ab] Kai Zhang,*[d] Tao Chen,[abe] Yunan Wang*[f] and Wei Lu*[abe]

Intelligent luminescent materials for rewritable and programmable information display have long been expected to be used to address potential environmental concerns stemming from the extensive use of disposable displays. However, most reported luminescence-colour changeable examples are chemically responsive and not well programmed to sequentially deliver different information within a single system. Additionally, they may suffer from residual chemical accumulation caused by the repeated addition of chemical inks and usually have poor rewritability. Herein, we draw inspiration from the bioelectricity-triggered information display mechanism of chameleon skin to report a robust electrothermally powered polymer gel actuator consisting of one soft conductive graphene/PDMS film and one humidity-responsive fluorescence-colour changeable CD-functionalized polymer (PAHCDs) gel layer. Owing to the good electrocaloric effect of the bottom graphene film and excellent hygroscopicity of the top PAHCDs gel layer, the as-designed actuator could be facilely controlled to exhibit reversible and synergistic 3D-shape/fluorescence-colour changeable behaviours in response to alternating electricity and humidity stimuli. On this basis, robust rewritable information display systems are fabricated, which enable not only on-demand delivery of written information, but also facile rewriting of lots of different information by the synergization of electroheat/humidity-triggered local 3D-deformation and fluorescence-colour changes. This work opens new avenues of research into rewritable information display and potentially inspires the future development of intelligent luminescent materials.

New concepts

Although great progress in intelligent luminescent materials for rewritable information display has been achieved, it remains a great challenge to realize residual-free reversible colour changes for rewritable information coding/decoding and programmable control of the written information to achieve a promising "multiple-output" display feature within a single system. Inspired by the bioelectricity-controlled synergistic discoloration/deformation behaviour of chameleon skin to enable reversible and programmable information delivery to their coexisting organisms, we develop novel electroheat/humidity-responsive polymer gel actuators. These actuators contained a new kind of humidity-responsive fluorescence-colour tunable polymeric gel layer with self-healing ability and a graphene/PDMS film with good electrocaloric effect, and thus could show reversible fluorescence-colour/shape change in response to alternating humidity and electroheat stimuli. Owing to the residue-free nature of the finely controllable electric stimulus and clean humidity stimulus, the actuator could be elaborately designed to serve as a rewritable information display platform for reversible and programmable information delivery. This work represents an important advance towards the development of luminescent rewritable information display materials. Considering the modular design principle of the multilayer-structure material design strategy, this proof-of-concept demonstration is expected to inspire more intelligent actuating materials and luminescent display systems in the near future.

Introduction

In the modern age of information explosion, the demands for secure information storage and on-demand delivery are

[a] *Key Laboratory of Marine Materials and Related Technologies, Zhejiang Key Laboratory of Marine Materials and Protective Technologies, Ningbo Institute of Materials Technology and Engineering, Chinese Academy of Sciences, Ningbo 315201, People's Republic of China. E-mail: luwei@nimte.ac.cn*
[b] *School of Chemical Sciences, University of Chinese Academy of Sciences, 19A Yuquan Road, Beijing 100049, People's Republic of China*
[c] *College of Materials Science and Engineering, Taiyuan University of Technology, Taiyuan 030024, People's Republic of China*
[d] *Sustainable Materials and Chemistry, Department of Wood Technology and Wood-based Composites, University of Göttingen, Göttingen 37077, Germany. E-mail: shaohuang.chen@forst.uni-goettingen.de, kai.zhang@uni-goettingen.de*
[e] *College of Material Chemistry and Chemical Engineering, Key Laboratory of Organosilicon Chemistry and Material Technology Ministry of Education, Hangzhou Normal University, Hangzhou 311121, People's Republic of China*
[f] *Zhejiang Key Laboratory of Advanced Fuel Cells and Electrolyzers Technology, Ningbo Institute of Materials Technology and Engineering, CAS, 1219 Zhongguan Road, Ningbo 315201, People's Republic of China. E-mail: wangyunan@nimte.ac.cn*

† Electronic supplementary information (ESI) available. See DOI: https://doi.org/10.1039/d4mh01172d

‡ These authors contributed equally.

increasing.[1] In this context, much recent research interest has been attracted to the development of rewritable information display systems, which are believed to reduce the cost of data storage media and reduce potential environmental concerns stemming from the extensive use of disposable or transient display systems.[2] Smart optical materials, which are capable of showing reversible optical changes in response to external stimuli, are promising candidates for the development of such rewritable visual information display systems.[3,4] Compared with common pigment/structure colour-changing materials such as dyes[5–10] and photonic crystals,[11–13] smart fluorescent materials are especially attractive for secure information display and transmission, because the written information is not only usually invisible in natural light, but also can be sophisticatedly encoded in multiple dimensions (*e.g.* intensity, wavelength or emission time).[14–18] Therefore, a wide variety of fluorescent material-based rewritable display systems have been developed rapidly in recent decades.[19] However, most of them, albeit state-of-the-art, are based on the covalent molecular structure transformations or noncovalent supramolecular assembly structure changes of the introduced fluorophores in response to chemical stimuli (*e.g.* organic solvent,[20,21] acid/base[22–25] or metal ions[26]), and thus usually operationally inconvenient. For example, it is usually impractical for untrained consumers to use acid, base or other chemical inks to write/erase certain information by themselves.[14] More importantly, since the repeated addition of chemical inks is usually required for the reversible chemical structure and fluorescence changes,

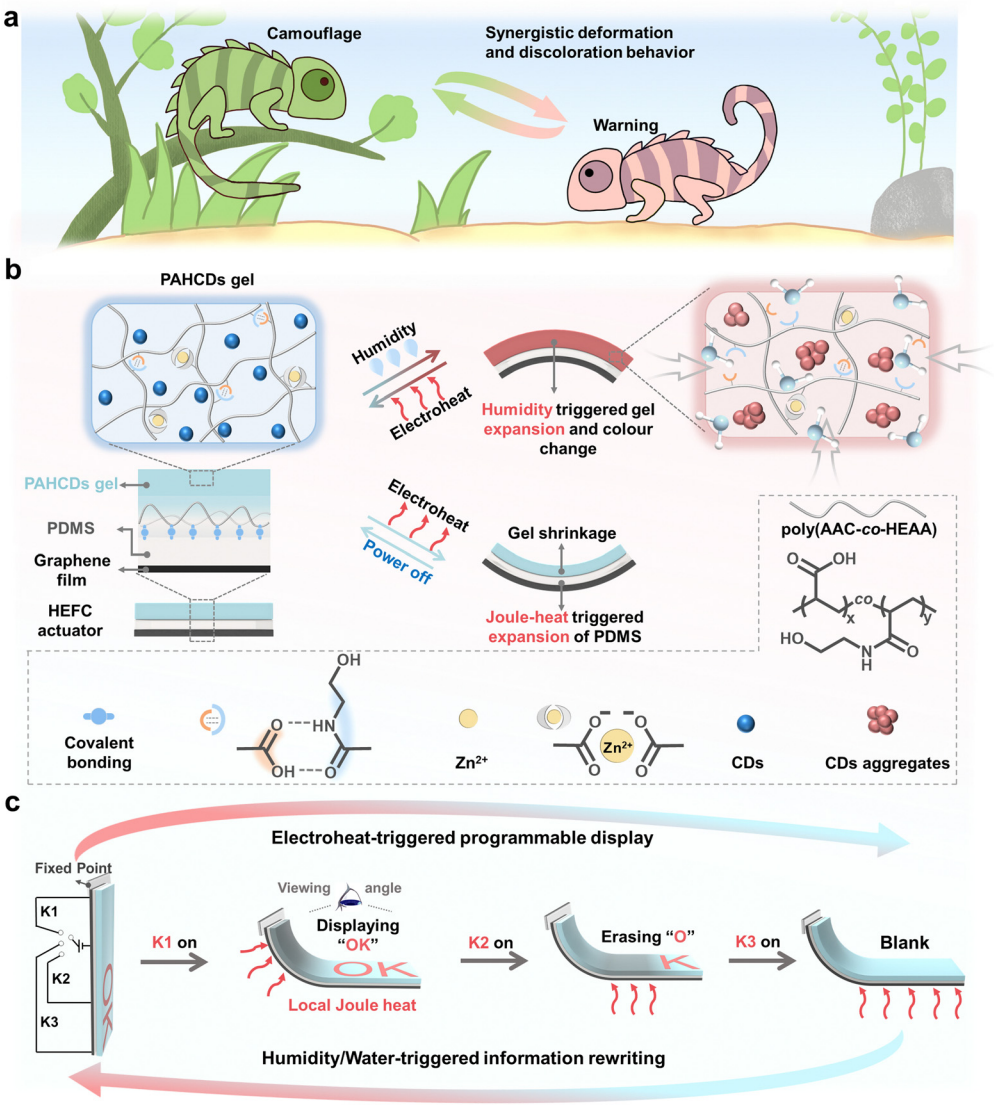

Scheme 1 Design of the humidity- and electroheat-responsive fluorescence-colour changeable (HEFC) polymer gel actuator. (a) Illustration showing the synergistic shape/colour-changing behaviour of chameleons for camouflage and warning. (b) Design of the fluorescent polymer gel actuator and its humidity- and electrothermal responsive synergistic fluorescence-colour/3D-shape changes and (c) its application for rewritable and programmable information display. PAHCDs gel is short for humidity-responsive fluorescence-colour changeable CDs-functionalized polymer gel; PDMS, AAc and HEAA stand for polydimethylsiloxane, acrylic acid and *N*-(2-hydroxyethyl)acrylamide, respectively.

these chemical-responsive systems easily suffer from residual chemical accumulation, which makes them usually have limited information rewritability.

In comparison, light/electricity/heat/water-responsive fluorescent systems seem more appealing in terms of rewritable information display uses, as these stimuli can be not only operationally facile, but also completely erased to facilitate another data rewriting/erasing cycle.[27–31] Taking electricity and water stimuli as examples, electrical signals show many advantages including popularity (easy to achieve in daily life), environmental friendliness, remote controllability and high tunability in terms of duration and amplitude,[32] while a water stimulus is fresh and clean, making it very attractive to be used as ink for information writing.[33] Therefore, it would be ideal if electricity and water stimuli were combined to trigger reversible colour changes of luminescent materials for rewritable information coding/decoding. However, related studies, despite the great potential, remain underdeveloped.[34,35] In addition, there is great interest in achieving the promising but rare ''multiple-output'' display feature within one display system, because such systems can be potentially programmed to convey different information by facilely varying one or two stimuli.[36] Therefore, it is still a challenge to develop more advanced electricity/water-responsive fluorescent materials that enable rewritable and programmable 3D-encoding information display.

Astonishingly, the merits of such rewritable and programmable information display are found to be combined in natural chameleon skin. Biological studies reveal that multi-layered chromatophores ringed by muscular cells exist in chameleon skin.[37] They have evolved to use a bioelectricity signal (nerve impulse) to trigger differential muscular movements around different chromatophores, which are then manifested as dynamic and reversible skin colours/patterns to enable efficient information delivery (*e.g.*, communication, camouflage and warning) to their co-existing organisms in their living environment. Chameleons can further synergize the bioelectricity-controlled simultaneous skin colour and 3D body gesture changes to further enhance the intelligence and programmability of information transmission, enabling them to better adapt to dynamic living environments (Scheme 1a).[38,39] Inspired by this phenomenon, we herein propose the development of humidity- and electroheat-responsive fluorescence-colour changeable (HEFC) polymer gel actuators, followed by the demonstration of 3D-encoding information carriers with rewritable and programmable display capacities. As illustrated in Scheme 1b, the polymer gel actuator was prepared by the covalent bonding of a soft conductive graphene/PDMS film and fluorescence-colour changeable poly(acrylic acid-*co*-*N*-hydroxyethylacrylamide) (poly(AAC-*co*-HEAA)) glycol gel functionalized with hydrophobic carbon dots (PAHCDs). Since the well-dispersed hydrophobic CDs were blue luminescent in glycol but gradually turned into red-light-emitting aggregates after being exposed to a high humidity environment, the PAHCDs gel showed a humidity-triggered blue-to-red fluorescence-colour change. When applying moisture stimulation to the actuator, the PAHCDs glycol gel layer would expand accompanied with blue-to-red emission colour change, leading to synergistic shape/colour changeable behaviour of the whole actuator. Upon further voltage input on the bottom conductive graphene layer, Joule heat was immediately generated and transmitted to the middle PDMS sheet and top PAHCDs gel. As a consequence, the PDMS layer was made to expand and the PAHCDs gel layer was triggered to shrink, resulting in electrothermally powered simultaneous fluorescence colour change and shape deformation recovery. On this basis, rewritable 3D-encoding information carriers were demonstrated, which enabled repeatable and programmable information delivery by synergistically utilizing water as ink for data writing and the electrothermally powered 3D shape/fluorescence-colour change for information display (Scheme 1c).

Results and discussion

Preparation of humidity-responsive fluorescence-colour changeable PAHCDs gels with self-healing ability

The humidity-responsive fluorescent carbon dots (PAHCDs) gels were prepared by photo-polymerizing a glycol solution of acrylic acid (AAC) and *N*-(2-hydroxyethyl)acrylamide (HEAA) in the presence of zinc acetate and AIE-active hydrophobic carbon dots (CDs). Herein, AAC was chosen as the primary monomer for gel synthesis owing to the superb water-absorbing capacity of poly(acrylic acid). Owing to the absence of any chemical cross-linkers, a small quantity of HEAA (molar ratio of AAC/HEAA $\sim$3.7) was employed as the co-monomer to introduce additional hydrogen-bonded crosslinks. As a result, poly(AAC-*co*-HEAA)glycol gel with good mechanical stress was produced, which was supposed to be densely crosslinked by the Zn^{2+} coordination and hydrogen bonding interactions. The noticeable peak shift of amide C=O groups from 1626 cm^{-1} to 1620 cm^{-1} could demonstrate the formation of Zn^{2+}–O=C coordinated interactions in the as-prepared PAHCDs gel (Fig. S1, ESI†). Since only the CDs contained the S element, the result of SEM elemental mapping by energy-dispersive X-ray spectroscopy (EDS) showed the even distribution of these fluorescent CDs in the PAHCDs gel (Fig. S2, ESI†), suggesting its quite good composition homogeneity. The water absorption rate of the PAHCDs-0.50 gel was first investigated under both normal (75% RH) and extreme (98% RH) conditions. It was found that the PAHCDs-0.50 gel could still absorb water molecules from the normal atmosphere (75% RH) and extreme environment (98% RH) to reach 120% and 160% of its original weight over 10 h at room temperature (Fig. S3, ESI†). These results further demonstrated the superb water-absorbing capacity of the polymeric gel matrix. As shown in Fig. 1a, the as-prepared PAHCDs gel initially exhibited blue fluorescence emission under 365-nm UV light, which gradually changed to red emission after exposure to high relative humidity (98%) within 60 min. This is because the AIE-active hydrophobic CDs exhibited blue dispersed emission in the good solvent glycol, but became gradually aggregated when water was introduced, thus leading to red aggregation-induced emission

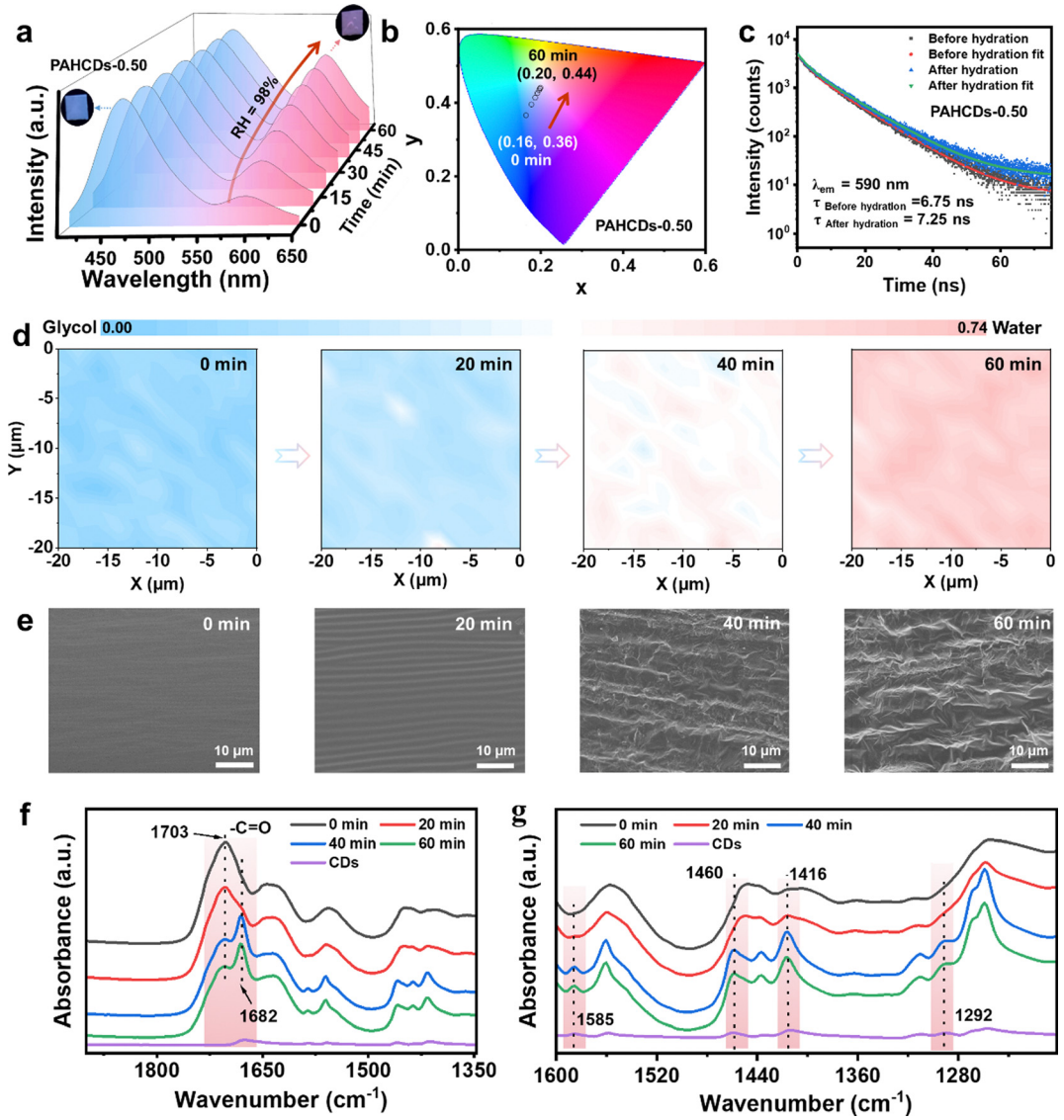

Fig. 1 Fluorescence responses of the PAHCDs-0.50 gel sample. (a) The fluorescence spectra of the PAHCDs-0.50 gel recorded at different time intervals after exposure to relative humidity (RH) of 98%. (b) Fluorescence colour change of the PAHCDs-0.50 gel before and after exposure to RH of 98% for 60 min shown on a CIE (1978) chromaticity diagram. (c) Fluorescence decay curves of the PAHCDs-0.50 gel before and after hydration under an excitation wavelength of 320 nm. (d) Raman mappings of the PAHCDs-0.50 gel surface recorded at different time intervals after exposure to RH of 98% for different times. The colour represents the Raman band ratio (I_{O-H}/I_{C-H}), and the red colour signifies higher I_{O-H}/I_{C-H} values. Cross-section SEM images (e) and FT-IR spectra (f) and (g) of the PAHCDs-0.50 gel sample exposed to RH 98% for different times.

(Fig. S4, ESI†). This remarkable fluorescence-color change is attributed to the π–π stacking interactions of carbonized cores and restriction of the surfaces' intramolecular rotation around disulfide bonds.[40] Considering that the fluorescence colour of the PAHCDs gel and its humidity-responsive fluorescence-colour-changeable ability largely depended on the aggregation extents of the CDs, PAHCDs gel samples containing different dosages of CDs were prepared and subjected to systematic photophysical studies. As shown in Fig. S5–S7 (ESI†), with an increase of the CDs content (f_{CDs}) from 0.17 to 0.50 wt%, all the PAHCDs gels were initially blue-light-emitting but exhibited an increased fluorescence-colour changing range after exposure to RH 98% for 60 min. As summarized in Fig. S7 (ESI†), it was found that the fluorescence intensity ratio (I_{590}/I_{465}) of the PAHCDs-0.50 (f_{CDs} = 0.50 wt%) gel sample increased from 0.23 to 0.74, while that of the PAHCDs-0.17 (f_{CDs} = 0.17 wt%) and PAHCDs-0.33 (f_{CDs} = 0.33 wt%) gels only enhanced from ~0.07 to ~0.28. Such a blue-to-red fluorescence colour change process of the PAHCDs-0.50 gel sample could be visually observed in the Commission Internationale de L'Eclairage (CIE) coordinate figure (Fig. 1b). Meanwhile, the PAHCDs-0.17 and PAHCDs-0.33 gels still exhibited blue emission after being treated under 98% RH for 60 min (Fig. S8 and S9, ESI†). These results suggested the formation of more CD aggregates in the PAHCDs-0.50 gel during the process of moisture absorption, and thus the PAHCDs-0.50 gel sample

possessing better colour-changing ability was chosen for the following studies.

To obtain more insight into the humidity-sensitive fluorescence colour-changing process, we investigated the fluorescence decay curves of the PAHCDs-0.50 gel before and after exposure to 98% RH under an excitation wavelength of 320 nm. As shown in the comparison in Fig. 1c and Fig. S10 (ESI†), its average fluorescence lifetime at 590 nm (red emission) increased from 6.75 ns to 7.25 ns at the cost of the lifetime at 465 nm (blue emission), which reduced from 3.31 ns to 2.51 ns after exposure to RH of 98% for 60 min. These results indicated that the dispersed hydrophobic CDs in the PAHCDs-0.50 gel were indeed aggregated as the hygroscopic process proceeded, thus resulting in the fluorescence colour change from blue to red. Additionally, *in situ* Raman mapping was carried out to further intuitively clarify this colour-changing process. Considering that ethylene glycol in the polymeric gel has both O–H and C–H bonds, while the absorbed water has only O–H bonds, the Raman intensity ratio of I_{O-H} to I_{C-H} (I_{O-H}/I_{C-H}) could be used to monitor the real-time moisture absorption process.[41] Specifically, I_{O-H} and I_{C-H} were respectively the integral areas of the stretching vibrations of O–H bonds at 3160–3500 cm^{-1} and C–H bonds at 2840–3030 cm^{-1}. As shown in Fig. S11 (ESI†), the Raman spectra of the PAHCDs-0.50 gel demonstrated significantly enhanced I_{O-H}/I_{C-H} after being placed under RH of 98% for 60 min, which was consistent with the *in situ* Raman mapping result that a higher I_{O-H}/I_{C-H} signal was recorded with increased exposure time under RH of 98% (Fig. 1d). These results indicated that a large amount of water had been adsorbed onto the gel surface to induce the aggregation of hydrophobic CDs, thus leading to fluorescence-emission change from blue to red. More evidence for this moisture adsorption process were deduced from the cross-sectional SEM images of a freeze-dried gel sample and after exposure under 98% RH at different time intervals, as well as the time-dependent Fourier transform infrared (FT-IR) spectra. With prolonged exposure time, the loosely connected porous structures of the PAHCDs gels were increasingly obvious (Fig. 1e), while the characteristic band intensity around 1682 cm^{-1} for the bonded C═O groups increased as a cost of the intensity for free C═O groups at 1703 cm^{-1} (Fig. 1f).[33,42] These results demonstrated that water molecules were indeed absorbed inside the gel to break the original H-bonding crosslinks by forming more new H-bonds between C═O and water molecules. Moreover, the formation of more CD aggregates in the PAHCDs-0.50 gel during the moisture absorption process was demonstrated by comparing the FT-IR spectra of the original CDs and gel sample. As shown in Fig. 1g and Fig. S12 (ESI†), the signals for C═C (1460 cm^{-1}), C–N (1416 cm^{-1}), C–NH (1292 cm^{-1}) and C–S (685 cm^{-1}) functional groups existing on the surface of the CDs were increasingly obvious in the FT-IR spectra of the PAHCDs-0.50 gel sample over time, indicating that more CD aggregates were being formed during the moisture absorption process. It was such CD aggregation that resulted in the blue-to-red fluorescence colour change owing to the AIE feature of the CDs.[40] Then, the red fluorescence of the PAHCDs-0.50 gel with water absorbed could almost recover to the initial blue after heating at 50 °C for 6 min to evaporate water (Fig. S13, ESI†). Also, with the increase of heating time, the fluorescence intensity ratio (I_{590}/I_{465}) of the PAHCDs-0.50 gel decreased from 0.74 to 0.31 (Fig. S14, ESI†).

The mechanical and self-healing properties of the PAHCDs-0.50 gel were further investigated. As shown in Fig. 2a, the gel exhibited a maximum tensile strength of ~400 kPa and a maximum tensile strain of ~1500%. Such a mechanical performance should originate from its multiple crosslinked polymer networks *via* supramolecular hydrogen bonding and metal coordination interactions, as well as the plasticizing effect of glycol solvent.[43] Additionally, the PAHCDs-0.50 gel was proved to be intrinsically self-healable because of its entirely supramolecular crosslinked polymer networks. As shown in Fig. 2c, the heart-shaped gel was first cut into two pieces and then self-healed together after being exposed to a high humidity environment (RH of 98%) at room temperature for 40 min. The optical images demonstrated that the border gradually disappeared and nearly vanished at room temperature for 1 h, indicating its satisfactory self-healing ability. The self-healing efficiency, which is defined as the ratio between the tensile stress of the self-healed sample and that of the original gel sample, could reach up to 80% after placement in a RH 98% environment for 12 h (Fig. 2a). Meanwhile, the facture strain, toughness and elastic modulus of the self-healed gel were measured to be mostly recovered (Fig. 2b). Additionally, rheological tests were carried out to further testify the favourable mechanical and self-healing properties of the PAHCDs-0.50 gel. As shown in Fig. 2e the rheology analysis showed the viscoelastic properties of the PAHCDs gel, which exhibited a dependence of G' and G'' on the percentage of applied strain ($\gamma > 10\%$), verifying gel formation. In addition, the strain alternation test showed viscoelasticity recovery of the PAHCDs-0.50 gel (Fig. 2e). The gel remained elastic (*i.e.* $G' > G''$) when initially placed under a low strain of 0.1% at room temperature for 100 s. Upon applying a high strain (γ = 300%) for 100 s, the gel became viscous (*i.e.*, $G'' > G'$). Notably, after reducing the strain back to 0.1% (for 180 s), the gel promptly healed within 15 s, almost recovering to its initial viscoelastic state. The alternating strain measurement could be repeated at least four times. These results further suggested the good self-healing properties of the PAHCDs-0.50 gel.[44]

Fabrication of humidity- and electroheat-responsive soft actuators with synergistic discoloration/deformation abilities

HEFC soft actuators with synergistic discoloration/deformation abilities were then fabricated by *in situ* synthesis of the fluorescence-colour changeable PAHCDs gel onto one soft electrothermal layer. As illustrated in Fig. S15 (ESI†), the soft electrothermal layer was obtained by transferring stacked graphene films self-assembled on a water/air interface onto a thin PDMS sheet (thickness ~200 μm). Closely packed graphene sheets endowed these films with outstanding conductive properties, which contributed to the high electrothermal conversion efficiency through the Joule heat effect (Fig. S16, ESI†).[32]

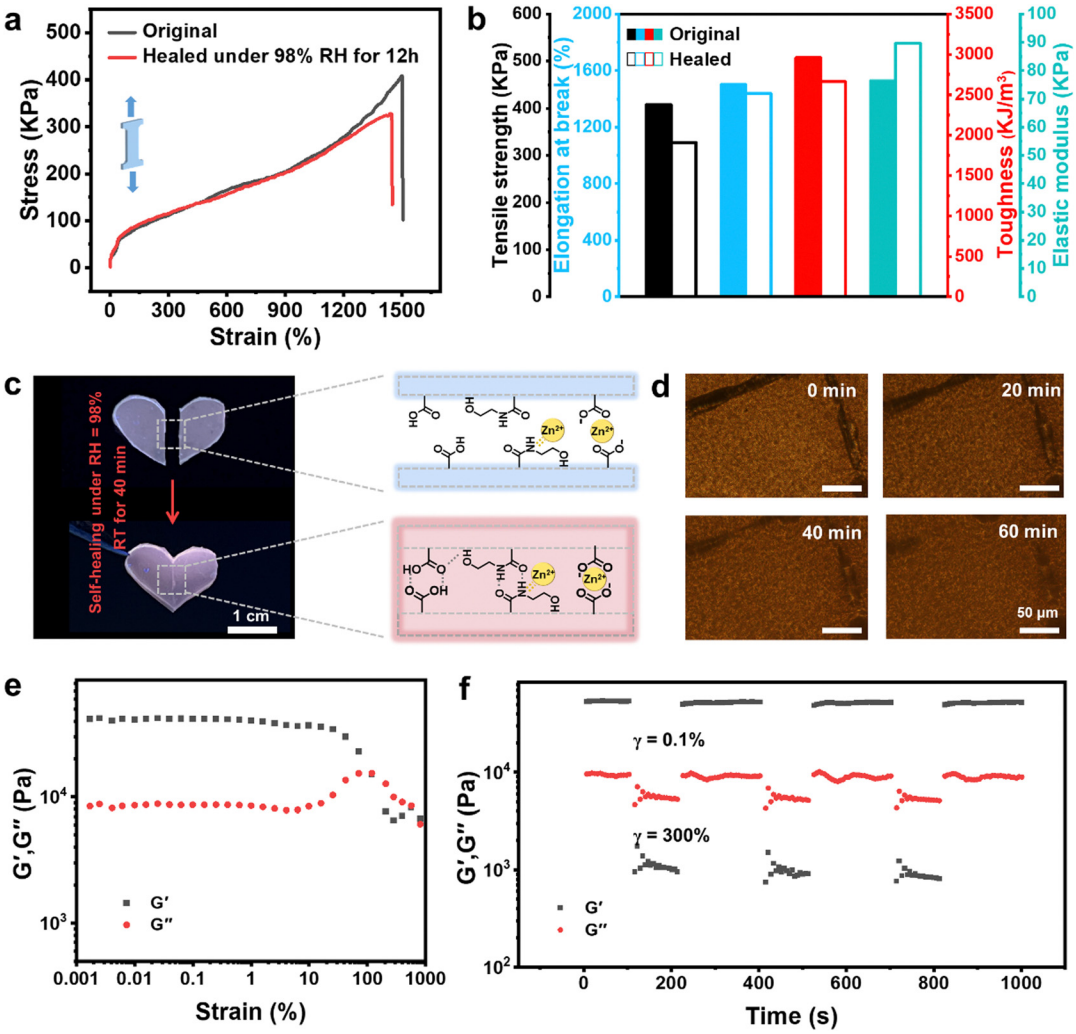

Fig. 2 The mechanical and self-healing properties of the PAHCDs-0.50 gel sample. (a) and (b) Stress–strain curves and several important mechanical properties of the original and self-healed PAHCDs-0.50 gels. (c) Photos showing the self-healing process of the PAHCDs-0.50 gel at room temperature (RT) and the proposed self-healing mechanism. (d) Microscopic images of the self-healing process. (e) Strain sweep test of the PAHCDs-0.50 gel (angular frequency 1 Hz). (f) Rheological strain recovery test of the PAHCDs: G' (black ■) and G'' (red ●) values of the PAHCDs-0.50 gel at a fixed angular frequency of 1 Hz. Strain percentage values (γ) are indicated.

In order to ensure stable interfacial bonding between the fluorescent gel layer and electrothermal layer, the PDMS sheet was first treated with air plasma, and sequentially immersed into a mixed solution ($V_{H_2O}:V_{HCl}:V_{H_2O_2}$, 5 : 1 : 1) and another mixed solution ($V_{Water}:V_{Ethanol}$, 1 : 1) containing 2 wt% 3-(trimethoxysilyl)propyl methacrylate (TMSPMA) to produce surface vinyl groups.[45] The precursor solution of the PAHCDs gel was placed onto the surface of the vinyl-modified PDMS sheet and *in situ* copolymerized to obtain the multilayer-structured HEFC actuator. Its interfacial multilayer structure could be clearly observed in the cross-section scanning electron microscope (SEM) image in Fig. 3a, showing that these layers were tightly integrated without gaps. In addition, a 90° peeling-off experiment was conducted to assess the interfacial adhesive force per length between the PAHCDs gel and PDMS sheet (Fig. 3b). It was found that the adhesive force reached up to 100 N m^{-1}, confirming that the interfacial bonding was strong enough to ensure stable actuation performance of the HEFC actuator. Electroheat-responsive actuation of the HEFC actuator was then investigated. As shown in Fig. 3c, the straight HEFC actuator with one end fixed was initially upright. Upon applying a voltage, the graphene film of the soft electrothermal layer would convert electricity into Joule heat *via* the electrocaloric effect. Then, the generated Joule heat was instantly transferred to the PDMS and PAHCDs gel layers, resulting in the expansion of the PDMS layer due to its high thermal expansion coefficient (about 250–300 × 10^{-6} K^{-1}),[46] and the contraction of the PAHCDs gel owing to gradual water evaporation. Therefore, the HEFC actuator would bend toward the PAHCDs gel side. Such electroheat-responsive reversible bending/unbending behavior of the multilayer-structured HEFC actuator should be primarily caused by the water dehydration and rehydration of the polymeric gel layer for the following reasons. The glass transition temperature of the dried gel polymer was measured to be about 56 °C (see the Fig. S17,

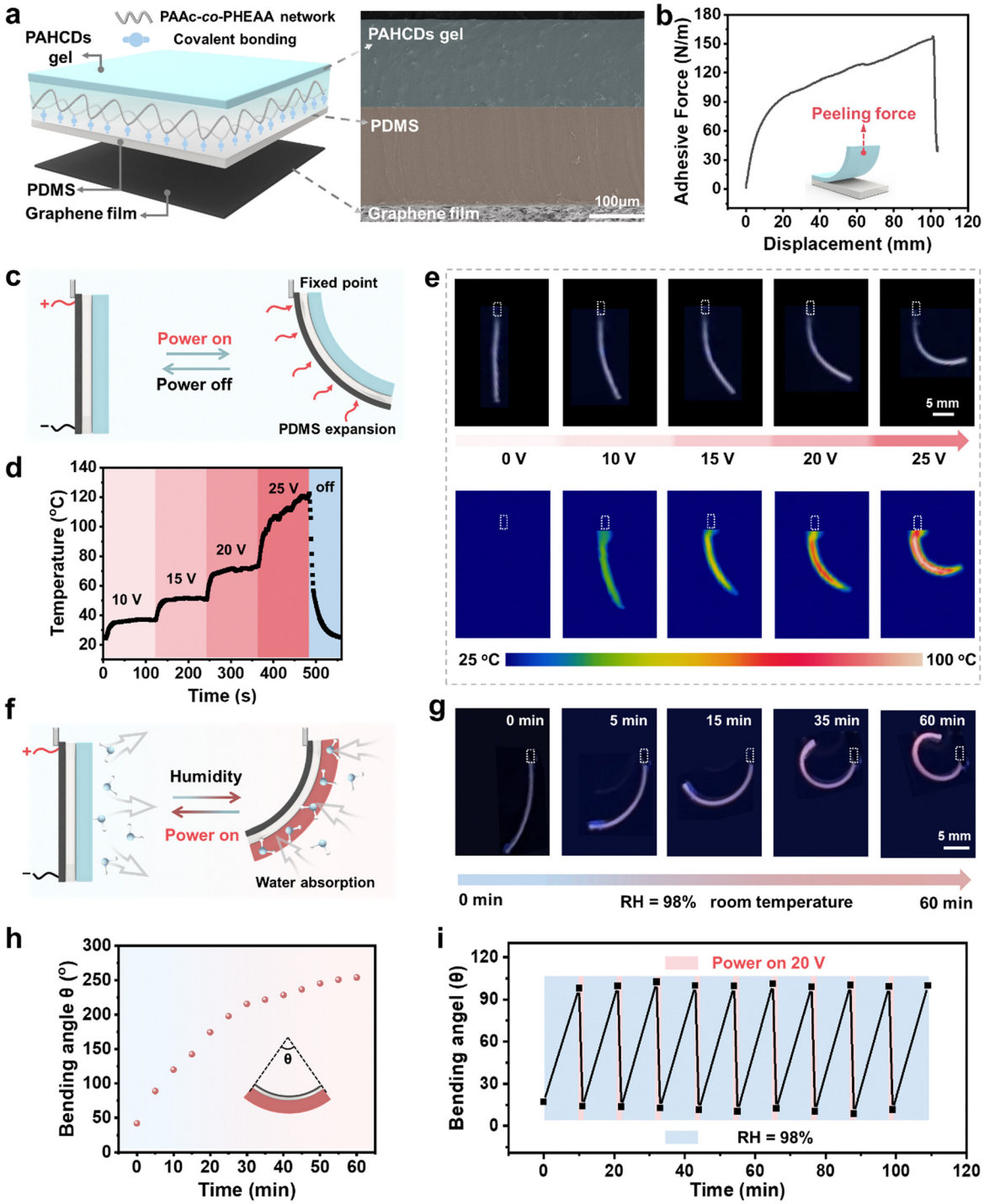

Fig. 3 Structure and working principle of the HEFC actuators. (a) Illustration and cross-section SEM image of the actuator. (b) Interfacial adhesive force per length between the PAHCDs-0.50 gel and PDMS, measured by standard 90° peel tests. (c) Illustration showing the electrothermally responsive deformation mechanism of the HEFC actuator. (d) The temperature recorded on graphene films of HEFC actuators with increasing voltage input. (e) Photos and corresponding IR images showing the electrically controlled shape changeable process of the actuator upon the input of different voltages. (f) Illustration and (g) photos showing the humidity/electroheat-triggered synergistic shape deformation and fluorescence colour changing process of the HEFC actuator. (h) The bending angles, θ, of the HEFC actuators as a function of the time exposed to RH of 98%. (i) Cyclic actuation of the HEFC actuator in response to alternating electricity (20 V voltage) and humidity stimuli. All photos were taken under 365 nm UV light.

ESI†). Additionally, the gel layer was known to have no phase transition behavior with increasing temperature. Therefore, when the voltage was applied to heat the polymer gel layer, there should be no noticeable heat-activated polymer conformation changes of the gel layer. Nevertheless, such high electro-heat would cause water molecules to gradually

evaporate from the gel matrix over time, leading to remarkable water dehydration of the gel layer and noticeable 3D shape deformation of the whole actuator.

Considering that the Joule heat generated by the graphene film was positively related to the applied voltage, it was expected that the surface temperature of the HEFC actuator could be facilely adjusted by tuning the magnitude of the applied voltage. As shown in Fig. 3d, upon gradually increasing voltage from 0 V to 25 V, the surface temperature on the graphene side of the HEFC actuator could be increased from ~24.2 °C to ~36.9 °C (10 V), 51.6 °C (15 V), ~72.1 °C (20 V) and even ~120.6 °C (25 V) within 120 s. Additionally, the temperature could also quickly decrease from ~120.6 °C to ~25.2 °C within 70 s after switching off the voltage. As expected, the bending angles changed incrementally from ~0° to ~132° after the applied voltage was increased from 0 V to 25 V (Fig. 3e and Fig. S18, ESI†). When the voltage was turned off, the gel layer would absorb water molecules from the surrounding atmosphere at room temperature to partially recover the actuated curvature owing to the superb water-absorbing capacity of the gel matrix. Quantitatively speaking, the bending angle was decreased from 57.7° to 31.6° after the 15 V voltage was turned off for 60 s, while the bending angle was decreased from 131.8° to 103.2° after the 25 V voltage was turned off for 60 s (Fig. S19, ESI†). These results suggested that the bending angles of the HEFC actuators could be facilely and continuously manipulated *via* the alteration of the applied voltage.

Next, interesting synergistic discoloration/deformation of the HEFC actuators was reversibly achieved in response to environmental humidity and electro-heat stimuli. As shown in Fig. 3f and g, the blue-light-emitting actuator was initially suspended with one end fixed under ambient conditions. When the relative humidity of the surrounding environment was increased to RH = 98%, the humidity-responsive PAHCDs gel side showed gradual volume expansion along with blue-to-red fluorescence-colour change due to water absorption. Meanwhile, the volume of the PDMS/graphene sheet remained constant, thus causing the actuator to bend against the gel side. Fig. 3h shows that the bending angle gradually increased with exposure time and reached above 250° within 60 min. It is worth noting that both the shape deformation and fluorescence-colour change were highly synchronous, because both processes were diffusion-controlled and activated by the same humidity stimulus. Upon subsequent voltage application, the whole actuator would be heated by Joule heat to evaporate water quickly, and recover to the initial blue fluorescent and upright state. As summarized in Fig. 3i, when the HEFC actuator was exposed to a high-humidity (RH = 98%) environment, it took 10 min to curve from ~0° to ~100°, but it only took 1 min to recover to ~0° when a 20 V voltage was applied. Such fast shape recovery was unexpected but easily understood, because the Joule heat not only caused rapid water evaporation of the gel layer, but also triggered instant thermal expansion of the PDMS layer. Such shape deformation of the multi-layered actuator that was accelerated by thermal expansion of the PDMS layer had been clearly demonstrated in our previous work as long as the temperature was above 40 °C.[47] Notably, it was further demonstrated that the humidity- and electroheat-responsive bending/recovery behaviours were reversible and could be repeated at least 10 times, suggesting its huge potential for use in rewritable information display (Fig. S20, ESI†).

Application of the HEFC actuators for rewritable and programmable information display

It is well known that some natural organisms such as chameleons are capable of displaying various body gestures to deliver distinct information to their coexisting organisms.[48] This finding further inspired us to utilize the above-established HEFC actuators to develop bio-inspired information delivery systems. Some studies recently found that it is a promising approach to produce actuators with complicated structures by endowing anisotropic materials with self-healing ability. These actuators enabled multimode actuation under as-designed stimuli to deliver substantial information.[49,50] As a proof-of-concept, the stimuli-responsive delivery of a variety of Morse code information was first demonstrated. As shown in Fig. 4a, the bending movements of the HEFC actuator towards the left and right side could be defined as dash (–) and dot (·) signals of Morse code, respectively. Meanwhile, the straight state was defined as "×", the blank signal (Fig. 4a). As such, the codes for 26 letters of the alphabet were interpreted as shown in the scheme in Fig. 4b. To demonstrate the responsive multiple information delivery potential, one integrated actuating system capable of showing multiple deformation states was designed (Fig. 4c) and fabricated by series-connecting four HEFC actuators by harnessing the self-healing capability of the PAHCDs gel layer (Fig. 4c_2). In the initial state, all four of the HEFC actuators (I–IV) were straight, representing the invalid "××××" information. Upon applying local moisture and/or electrical stimuli to different actuators of the system, different deformation states would be produced to transmit diverse messages. For example, when locally applying moisture to actuator I of this straight actuator, its PAHCDs gel layer would be swollen to make actuator I bend towards the left side, delivering the dash (–) signal of Morse code (Fig. 4c_2–c_1). Meanwhile, the other three actuators were kept straight. In this case, the Morse code signal of the system was recognized as "–×××", which could be decoded to the English letter "T" (Fig. 4c_1). It was noteworthy that the "T" information could be completely erased by applying a 15 V voltage to the graphene film layer of actuator I to trigger the dehydration-induced shape recovery (Fig. 4c_1–c_2) and subsequently allow the responsive delivery of another English letter. As shown from Fig. 4c_2–c_3, the recovered straight system could be reprogrammed to convey message "F" by locally applying the electricity stimulus to actuator I and moisture stimulus to actuator II–IV. Following a similar procedure, the letter "C" could be encoded by applying the moisture stimulus to all four actuators (Fig. 4c_2–c_4). The letter "A" could be encoded by applying a 15 V voltage to actuator I–II (Fig. 4c_2–c_5), while the letter "S" could be displayed by applying a 15 V voltage to actuator I and III, as well as a moisture stimulus to actuator II (Fig. 4c_2–c_6). In this way, information corresponding to almost

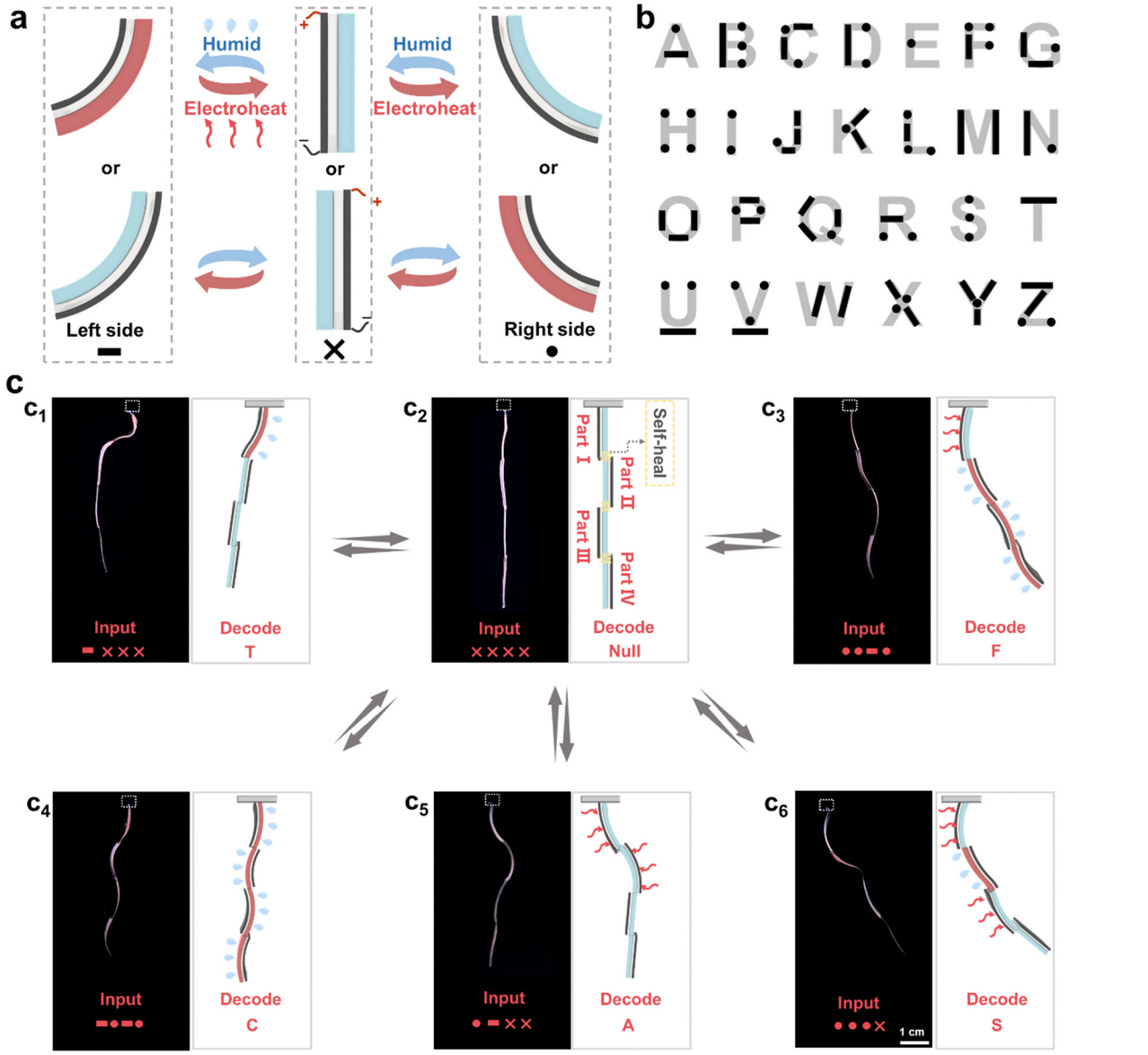

Fig. 4 Demonstration of the integrated HEFC actuating system for the rewritable and programmable display of Morse code. (a) Illustration showing the bending movements of the HEFC actuator towards left and right sides, which could be defined as dash (–) and dot (·) signals of Morse code, as well as the straight state that was defined as "×", the blank signal. (b) Representation of the alphabet in International Morse code. (c) Illustrations and photos showing the potential of the system to enable the programmable and reversible display of various Morse codes representing different English letters by synergizing local humidity and electro-heat stimuli.

all 26 English letters could potentially be delivered by this integrated actuating system. Importantly, information for every encoded letter could be reversibly erased to enable the display of information corresponding to another letter, suggesting its powerful potential for multiple information delivery.

Besides adjustable body shapes/gestures, chameleons can vary their skin colours/patterns.[39] Such environment-responsive synergistic 3D-shape/skin-colour changes are essential traits for their survival, enriching information delivery and communication with their partners or coexisting organisms. This further encouraged us to utilize the above-established HEFC actuators to construct environment-interactive rewritable information display systems. As can be seen from Fig. 5a, the red fluorescent letter "W" could be clearly written on the blank PAHCDs gel layer by using water ink and then totally erased by applying a 15 V voltage on the bottom graphene film layer to generate Joule heat for fast water evaporation. Owing to the unique "residue-free" nature of water and electro-thermal stimuli, other letters such as "R", "I", "T", "A", "B", "L" and "E" could be sequentially rewritten and erased, suggesting good rewritable information display capacity (Fig. 5a and Fig. S19, ESI†). To investigate the information duration time under ambient conditions, "CAS" letters and a heart-shaped figure were drawn on the gel surface by using water as ink. It was found that the water-written "CAS" letters and heart-

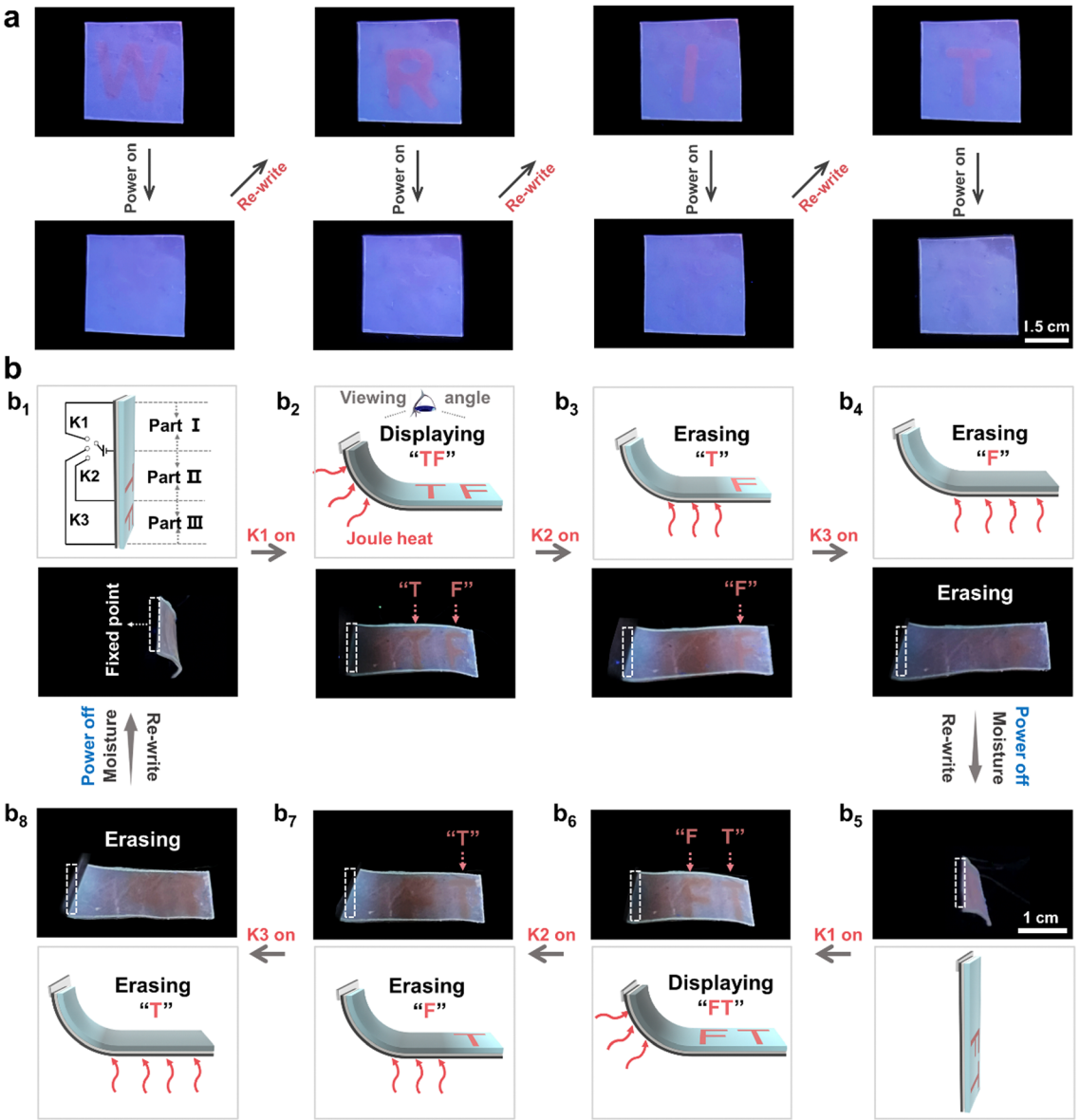

Fig. 5 Demonstration of the integrated HEFC actuating system for the rewritable and programmable display of different information. (a) Photos showing the information writing process by using water as ink and reversible information erasure by using electro-heat as the trigger. (b) Illustration and photos showing the potential of the system to enable the programmable and reversible display of a variety of information by synergizing local humidity/electro-heat stimuli to trigger synergistic shape deformation and fluorescence-colour changes. All photos were taken under 365 nm UV light.

shaped figure could be clearly maintained for 6 h under ambient conditions (26 °C, 60–70% RH), but gradually became illegible because too much water had been absorbed into the gel matrix to trigger blue-to-red fluorescence colour change of the whole gel sample. Note that when these absorbed water molecules were evaporated upon applying electrical power, other information could be re-written on the gel sample to enable rewritable information display (Fig. S21, ESI†).

To enhance the richness of rewritable information delivery, a proof-of-concept demonstration that synergized local 3D-deformation and fluorescence-colour variations was designed. Fig. 5b depicts its circuit design and basic structure, in which the stripe actuator with one end fixed was furnished with three electrical switches and two red fluorescent letters "TF" were written on the PAHCDs gel layer by using water ink (Fig. 5b$_1$). At the initial state shown in Fig. 5b$_1$, the stripe actuator was kept upright to hide the written "T" and "F" information from the observer's perspective. When K1 was turned on to apply a 5 V voltage to the graphene film layer beneath part I to trigger its bending, part II–III of the actuator would be lifted to make the written letters observable (Fig. 5b$_2$). Subsequently, upon shifting the electrical switch to K2, the letter "T" would be erased by the local Joule heat on part II (Fig. 5b$_3$). Further switching to K3 would connect part II–III into the circuit to generate local Joule heat for the stepwise erasure of the letter "F" (Fig. 5b$_4$). After turning off all switches, local moisture was

applied to part I to recover its straight and upright state to enable the rewriting and stepwise display of different information. As demonstrated in Fig. $5b_5$–b_8, we could rewrite red fluorescent "F" and "T" letters on the PAHCDs gel layer, and sequentially program these electrical switches to enable the stepwise display of "FT", "T" and nothing. In this way, environment-interactive rewritable information display systems that can synergize local 3D-deformation and fluorescence-colour changes to deliver a variety of information are demonstrated for the first time. This is believed to enrich the environment-interactive functions of soft actuators and promote the development of next-generation smart display systems.

Conclusion

Inspired by the bioelectricity-triggered capacity of chameleon skin to display different information within a single system *via* the simultaneous modulation of skin colour and body gestures, we developed a robust electrothermally powered synergistic fluorescence-colour/3D-shape changeable polymer gel actuator for rewritable and programmable information display. The actuator was designed to consist of a soft conductive graphene/PDMS film exhibiting an electrothermal effect and a humidity-responsive fluorescence-colour changeable polymeric (PAHCDs) gel layer with self-healing ability. Under the conditions of high relative humidity, the PAHCDs gel layer absorbed water to bend the actuator towards the graphene/PDMS layer, accompanied by a blue-to-red fluorescence-colour change. Upon further voltage application, the graphene film generates Joule heat to induce the volume expansion of the PDMS film layer and water evaporation of the PAHCDs gel layer, resulting in simultaneous 3D-shape and fluorescence-colour recovery of the whole actuator. On this basis, an integrated actuating system was designed by series-connecting and self-healing four HEFC actuators together, which could be programmed to show multiple 3D deformation states to convey many distinct Morse code letters by facilely controlling the electroheat/humidity stimuli. Furthermore, an environment-interactive rewritable information display system was demonstrated, in which water-written red fluorescent English letters could be sequentially erased by local Joule heat to enable the stepwise display of different messages and then completely erased to allow another information writing cycle. This work has demonstrated the possibility of synergizing local 3D-deformation and fluorescence-colour changes for the delivery of different information within a single system, and thus is expected to inspire more intelligent actuating materials and luminescent display systems in the near future.

Author contributions

K. Zhang, T. Chen, Y. Wang and W. Lu conceived the idea, and designed and supervised the research. J. Xie, C. Yue and S. Chen designed and performed the experiments, and analysed the data. Z. Jiang and S. Wu performed the chemical synthesis. W. Yang gave advice on measurements. All authors discussed the results, and wrote and revised the manuscript.

Data availability

The authors confirm that the data supporting the findings of this study are available within the article and/or its ESI.†

Conflicts of interest

There are no conflicts to declare.

Acknowledgements

This work was supported by Natural Science Foundation of China (52073297), Zhejiang Provincial Natural Science Foundation of China (LR23E030001), International Cooperation Project of Ningbo City (2023H019), and the Sino-German mobility program (M-0424). The authors also thanked Prof. Patrick Théato from the Karlsruhe Institute of Technology for his thoughtful suggestions. S. Chen thanks China Scholarship Council for supporting his joint PhD program.

Notes and references

1 J. Zhang, S. Qin, S. Zhang, C. Sun, Y. Ren, L. Zhang, J. Liu, J. Xiao, W. Hu, H. Yang and D. Yang, *Adv. Mater.*, 2024, **36**, e2305872.
2 S. Wei, W. Lu, H. Shi, S. Wu, X. Le, G. Yin, Q. Liu and T. Chen, *Adv. Mater.*, 2023, **35**, e2300615.
3 M. I. Khazi, W. Jeong and J. M. Kim, *Adv. Mater.*, 2018, **30**, e1705310.
4 Y. Sun, X. Le, S. Zhou and T. Chen, *Adv. Mater.*, 2022, **34**, e2201262.
5 L. Mao, Z. Wang, Y. Duan, C. Xiong, C. He, X. Deng, Y. Zheng and D. Wang, *ACS Nano*, 2021, **15**, 10384–10392.
6 G. Xi, L. Sheng, J. Du, J. Zhang, M. Li, H. Wang, Y. Ma and S. X. Zhang, *Nat. Commun.*, 2018, **9**, 4819.
7 F. Wang, A. Cui, Z. Hu and L. Zhang, *Adv. Opt. Mater.*, 2021, **9**, 2101505.
8 M. Wu, Y. Li, W. Yuan, G. De Bo, Y. Cao and Y. Chen, *J. Am. Chem. Soc.*, 2022, **144**, 17120–17128.
9 H. Ju, C. N. Zhu, H. Wang, Z. A. Page, Z. L. Wu, J. L. Sessler and F. Huang, *Adv. Mater.*, 2022, **34**, e2108163.
10 W. He, Y. Yuan, M. Wu, X. Li, Y. Shen, Z. Qu and Y. Chen, *Angew. Chem., Int. Ed.*, 2023, **62**, e202218785.
11 Y. Xie, Y. Meng, W. Wang, E. Zhang, J. Leng and Q. Pei, *Adv. Funct. Mater.*, 2018, **28**, 1802430.
12 L. Shang, W. Zhang, K. Xu and Y. Zhao, *Mater. Horiz.*, 2019, **6**, 945–958.
13 H. Tan, Q. Lyu, Z. Xie, M. Li, K. Wang, K. Wang, B. Xiong, L. Zhang and J. Zhu, *Adv. Mater.*, 2019, **31**, e1805496.
14 Z. Li, X. Liu, G. Wang, B. Li, H. Chen, H. Li and Y. Zhao, *Nat. Commun.*, 2021, **12**, 1363.
15 K. Lou, Z. Hu, H. Zhang, Q. Li and X. Ji, *Adv. Funct. Mater.*, 2022, **32**, 2113274.

16 H. Wang, X. Ji, Z. Li and F. Huang, *Adv. Mater.*, 2017, **29**, 1606117.
17 F. Yang, T. Geng, H. Shen, Y. Kou, G. Xiao, B. Zou and Y. Chen, *Angew. Chem., Int. Ed.*, 2023, **62**, e202308662.
18 Q. Guo, B. Huang, C. Lu, T. Zhou, G. Su, L. Jia and X. Zhang, *Mater. Horiz.*, 2019, **6**, 996–1004.
19 R. Lan, J. Bao, Z. Li, Z. Wang, C. Song, C. Shen, R. Huang, J. Sun, Q. Wang, L. Zhang and H. Yang, *Angew. Chem., Int. Ed.*, 2022, **61**, e202213915.
20 Y. Jiang, J. Ma, Z. Ran, H. Zhong, D. Zhang and N. Hadjichristidis, *Angew. Chem., Int. Ed.*, 2022, **61**, e202208516.
21 C. Sun, H. Lu, C. Y. Yue, H. Fei, S. Wu, S. Wang and X. W. Lei, *ACS Appl. Mater. Interfaces*, 2022, **14**, 56176–56184.
22 Y. Zhang, X. Le, Y. Jian, W. Lu, J. Zhang and T. Chen, *Adv. Funct. Mater.*, 2019, **29**, 1905514.
23 R. Wang, Y. Zhang, W. Lu, B. Wu, S. Wei, S. Wu, W. Wang and T. Chen, *Angew. Chem., Int. Ed.*, 2023, **62**, e202300417.
24 X. Le, H. Shang, H. Yan, J. Zhang, W. Lu, M. Liu, L. Wang, G. Lu, Q. Xue and T. Chen, *Angew. Chem., Int. Ed.*, 2021, **60**, 3640–3646.
25 C. Yang, H. Xiao, L. Tang, Z. Luo, Y. Luo, N. Zhou, E. Liang, G. Wang and J. Tang, *Mater. Horiz.*, 2023, **10**, 2496–2505.
26 J. Deng, H. Wu, W. Xie, H. Jia, Z. Xia and H. Wang, *ACS Appl. Mater. Interfaces*, 2021, **13**, 39967–39975.
27 J. Zhang, H. Shen, X. Liu, X. Yang, S. L. Broman, H. Wang, Q. Li, J. W. Y. Lam, H. Zhang, M. Cacciarini, M. B. Nielsen and B. Z. Tang, *Angew. Chem., Int. Ed.*, 2022, **61**, e202208460.
28 Z. Wang, Z. Zhang, L. Tao, N. Shen, B. Hu, L. Gong, J. Li, X. Chen and X. Huang, *Angew. Chem., Int. Ed.*, 2019, **58**, 9974–9978.
29 Y. Ma, P. She, K. Y. Zhang, H. Yang, Y. Qin, Z. Xu, S. Liu, Q. Zhao and W. Huang, *Nat. Commun.*, 2018, **9**, 3.
30 H. L. Liu, H. Y. Ru, M. E. Sun, Z. Y. Wang and S. Q. Zang, *Adv. Opt. Mater.*, 2021, **10**, 2101700.
31 Y. Ai, Y. Fei, Z. Shu, Y. Zhu, J. Liu and Y. Li, *Chem. Eng. J.*, 2022, **450**, 138390.
32 J. Xie, S. Wei, W. Lu, S. Wu, Y. Zhang, R. Wang, N. Zhu and T. Chen, *Small*, 2023, **19**, 2304204.
33 Y. Liu, B. Xu, S. Sun, J. Wei, L. Wu and Y. Yu, *Adv. Mater.*, 2017, **29**, 1604792.
34 B. Li, Y. Zhang, J. Wang, B. Yan, J. Liang, Y. Dong and Q. Zhou, *ACS Appl. Mater. Interfaces*, 2022, **14**, 49119–49127.
35 P. She, Y. Ma, Y. Qin, M. Xie, F. Li, S. Liu, W. Huang and Q. Zhao, *Matter*, 2019, **1**, 1644–1655.
36 B. Wu, M. Si, L. Hua, D. Zhang, W. Li, C. Zhao, W. Lu and T. Chen, *Adv. Mater.*, 2024, **36**, 2401659.
37 W. Lu, M. Si, X. Le and T. Chen, *Acc. Chem. Res.*, 2022, **55**, 2291–2303.
38 R. A. Ligon and K. J. McGraw, *Biol. Lett.*, 2013, **9**, 20130892.
39 G. F. Grether, G. R. Kolluru and K. Nersissian, *Biol. Rev. Cambridge Philos. Soc.*, 2004, **79**, 583–610.
40 H. Yang, Y. Liu, Z. Guo, B. Lei, J. Zhuang, X. Zhang, Z. Liu and C. Hu, *Nat. Commun.*, 2019, **10**, 1789.
41 S. Wu, H. Shi, S. Wei, H. Shang, W. Xie, X. Chen, W. Lu and T. Chen, *Small*, 2023, **19**, e2300191.
42 Z. Han, P. Wang, Y. Lu, Z. Jia, S. Qu and W. Yang, *Sci. Adv.*, 2022, **8**, eabl5066.
43 X. Duan, J. Yu, Y. Zhu, Z. Zheng, Q. Liao, Y. Xiao, Y. Li, Z. He, Y. Zhao, H. Wang and L. Qu, *ACS Nano*, 2020, **14**, 14929–14938.
44 S. Bhattacharya, R. S. Phatake, S. Nabha Barnea, N. Zerby, J. J. Zhu, R. Shikler, N. G. Lemcoff and R. Jelinek, *ACS Nano*, 2019, **13**, 1433–1442.
45 H. Lin, S. Ma, B. Yu, X. Pei, M. Cai, Z. Zheng, F. Zhou and W. Liu, *Chem. Mater.*, 2019, **31**, 9504–9512.
46 G. Zhang, Y. Sun, B. Qian, H. Gao and D. Zuo, *Polym. Test.*, 2020, **90**, 106670.
47 H. Shi, S. Wu, M. Si, S. Wei, G. Lin, H. Liu, W. Xie, W. Lu and T. Chen, *Adv. Mater.*, 2021, **34**, 2107452.
48 H. Lu, B. Wu, X. Le, W. Lu, Q. Yang, Q. Liu, J. Zhang and T. Chen, *Adv. Funct. Mater.*, 2022, **32**, 2206912.
49 J. Lou, Z. Liu, L. Yang, Y. Guo, D. Lei and Z. You, *Adv. Funct. Mater.*, 2021, **31**, 2008328.
50 H. Qin, T. Zhang, N. Li, H. P. Cong and S. H. Yu, *Nat. Commun.*, 2019, **10**, 2202.

